DIPARTIMENTO DI MATEMATICA
"Francesco Brioschi"
POLITECNICO DI MILANO

Analytical and Numerical Study of Photocurrent Transients in Nanoscale Organic Solar Cells

de Falco, C.; Sacco, R.; Verri, M.

Collezione dei *Quaderni di Dipartimento*, numero **QDD 53**
Inserito negli *Archivi Digitali di Dipartimento* in data 25-9-2009

Piazza Leonardo da Vinci, 32 - 20133 Milano (Italy)

Analytical and Numerical Study of Photocurrent Transients in Nanoscale Organic Solar Cells

[a] *Istituto di Matematica Applicata e Tecnologie Informatiche del C.N.R., via Ferrata 1, 27100, Pavia (Italy)*

[b] *Dipartimento di Matematica "F.Brioschi", Politecnico di Milano, via Bonardi 9, 20133 Milano Italy*

Carlo de Falco [a] Riccardo Sacco [b] Maurizio Verri [b]

Abstract

In this article, we deal with the mathematical modeling and numerical simulation of photocurrent transients in nanoscale mono-layer Organic polymer Solar Cells (OSCs). The mathematical model consists of a system of non-linear diffusion-reaction partial differential equations (PDEs) with electrostatic convection, coupled to a kinetic ordinary differential equation (ODE). We propose a suitable reformulation of the model which makes it similar to the classical drift-diffusion system for inorganic semiconductor devices. This allows us, on the one hand, to prove the existence of a solution for the problem in both stationary and transient conditions and, on the other hand, to better highlight the role of exciton dynamics in determining the device turn-on time. For the numerical treatment of the problem, we carry out a temporal semi-discretization using an implicit adaptive method, and the resulting sequence of differential subproblems is linearized using the Newton-Raphson method with inexact evaluation of the Jacobian. Then, we use exponentially fitted finite elements for the spatial discretization, and we carry out a thorough validation of the computational model by extensively investigating the impact of the model parameters on photocurrent transient times.

Key words: Organic photovoltaic devices; solar cells; reaction-diffusion systems with electrostatic convection; numerical simulation; finite element method.

1 Introduction and Motivation

A continuously growing attention has been paid over the last years by the international community and government authorities to monitoring the effect

of the increase of global concentrations of carbon dioxide, methane and nitrous oxide on the quality of our every day's life. Results on the investigation carried out by the Intergovernmental Panel on Climate Change (IPCC) are documented in a recent report [2], where it is shown that *i*) the increase in carbon dioxide, the most important greenhouse gas, is primarily due to fossil fuel use; and *ii*) the increased concentrations of carbon dioxide, methane, and nitrous oxide have increased the average global temperature, strongly contributing to the so-called "global warming".

Based on the aforementioned IPCC report, specific guidelines for governance of energy waste emissions and sustainable future have then been ruled out by the European Union (EU) in [15]. In this document, the EU has decided that carbon dioxide emissions should decrease by 20 percent and that 20 percent of the energy produced in EU should originate from renewable energy sources, such as wind, water, biomass, and solar, not later than 2020. According to these indications, research and design of third generation photovoltaic cells and devices [20] for solar energy conversion into electrical and thermal energy turns out to be a central topic in the wider area of renewable energy sources. Roughly speaking, presently studied photovoltaic devices can be divided into two main classes: organic cells [33,32,22] and electrochemical cells [19,18,4]. Most of investigation activity is devoted to the experimental study of innovative materials to be employed for efficient and flexible technologies, and is not presently accompanied by a systematic use of computational models that allows to predict and optimize their performance.

In this article, we focus on the mathematical study of a special, and relevant, class of OSCs, namely the Bulk Hetero-Junctions (BHJ), because they currently represent the most promising technology in the area due to their ability in maximizing the harvesting of photogenerated charge by mixing together the donor and acceptor materials into a single blended layer. A first objective of this article is to carry out a mathematical investigation of the charge transport model proposed in [25], to gain insight in the understanding of the performance of the OSC, especially in terms of its dependence on the main physical modeling parameters. As a matter of fact, the complexity of the nanostructured BHJ material reflects into a high complexity of the system equations, which consist of a set of non-linear PDEs of diffusion-reaction type with electrostatic convection coupled with a kinetic ODE describing the temporal evolution of exciton concentration in the cell, and strongly demands for an *a-priori* analysis of the problem solution. With this aim, under suitable assumptions on the model coefficients, *i*) we prove the existence of a solution of the problem in stationary conditions; and *ii*) we derive a simplified model in transient conditions, that is amenable for a qualitative analysis of the time response of the device, and for which we again prove existence of a solution. A second objective of this article is to develop and implement a robust numerical algorithm for the computer-aided-design of advanced OSCs in both

steady and time-dependent regimes. As a matter of fact, the computational experiments of [25] indicate that the response of an OSC to a sharp turn-on illumination, besides depending on carrier transport time, is significantly determined by both geminate and bimolecular recombination processes. The heavily non-linear interplay between these two-scale phenomena must, therefore, be properly accounted for, to allow an accurate and detailed description of the input/output behaviour of the device, even under extreme working conditions. With this aim, for the numerical treatment of the problem, we carry out a temporal semi-discretization using an implicit adaptive method, and the resulting sequence of differential subproblems is linearized using the Newton-Raphson method with inexact evaluation of the Jacobian. Then, we use exponentially fitted finite elements for the spatial discretization, in such a way to ensure a stable approximation of steep internal and boundary layers arising in the distribution profile of the photogenerated carriers in the OSC. Both mathematical model and computational tool are then subject to a thorough validation of the computational model by extensively investigating the impact of the model parameters on photocurrent transient times.

A brief outline of the article is as follows. In Sect. 2, we describe the mathematical model for organic solar cells; in Sect. 3, we carry out the analysis of existence of a solution of the model, in both stationary and transient regimes; in Sect. 4, we discuss the numerical formulation of the problem; in Sect. 5 we illustrate the performance of model and methods in the simulation of a realistic organic solar cell of nanoscale size; in Sect. 6 we address some concluding remarks and indicate possible future research directions.

2 The Mathematical Model

In this section, we illustrate the mathematical model, proposed and numerically investigated in [25], that is used to describe the photogeneration mechanisms that drive charge transport in BHJ solar cells. In view of the analysis of the existence of a solution and of the discretization of the problem, we prefer to present the system equations under a more general perspective than in [25], following the treatment and notation of [36,42,43].

Let Ω be a bounded domain in $\mathbb{R}^d$, $d \geq 1$, with a Lipschitz boundary $\Gamma \equiv \partial\Omega$ divided into two disjoint subregions, Γ_D and Γ_N, with $\mathrm{meas}(\Gamma_D) > 0$ and such that $\Gamma_D \cap \Gamma_N = \emptyset$, and denote by $\boldsymbol{\nu}$ the outward unit normal vector along Γ. Then, given any $T \in (0, +\infty)$, the initial-boundary value problem that we wish to solve in $\Omega_T \equiv \Omega \times (0, T)$ to mathematically study and predict the

macroscopic input/output behavior of the organic solar cell, reads:

$$\begin{cases} & -\mathrm{div}(\varepsilon \boldsymbol{\nabla}\varphi) & = \sum_{i=1}^{2} q_i u_i, \\ \dfrac{\partial u_i}{\partial t} & -\mathrm{div}\boldsymbol{J}_i(u_i;\boldsymbol{\nabla}\varphi) = G_i(\boldsymbol{\nabla}\varphi, X) - R_i(\boldsymbol{u})u_i, & i = 1,2, \\ \dfrac{\partial X}{\partial t} & & = g(\boldsymbol{u}) - r(\boldsymbol{\nabla}\varphi, X), \end{cases} \tag{1}$$

where $\boldsymbol{u} = [u_1, u_2]^T$, ε is the dielectric permittivity of the material constituting the cell, and $q_1 = -q$, $q_2 = +q$, $q > 0$ being the electron charge. Equations (1) are supplied with the following constitutive relations for the flux densities $\boldsymbol{J}_i$

$$\boldsymbol{J}_i = D_i(\boldsymbol{\nabla}\varphi)\boldsymbol{\nabla}u_i + \boldsymbol{v}_i(\boldsymbol{\nabla}\varphi)u_i, \tag{2}$$

and are subject to the following boundary and initial conditions:

$$\begin{cases} \boldsymbol{u} = \boldsymbol{U}, \quad \varphi = \Psi & \text{on } \Gamma_D \times (0,T), \\ \boldsymbol{J}_i \cdot \boldsymbol{\nu} = \boldsymbol{\nabla}\varphi \cdot \boldsymbol{\nu} = 0 & \text{on } \Gamma_N \times (0,T), \\ \boldsymbol{u}(\boldsymbol{x},0) = \boldsymbol{U}(\boldsymbol{x},0) & \text{for } \boldsymbol{x} \in \Omega, \\ X(\boldsymbol{x},0) = X_0(\boldsymbol{x}) & \text{for } \boldsymbol{x} \in \Omega, \end{cases} \tag{3}$$

where $\boldsymbol{U} = [U_1, U_2]^T$ and Ψ are given functions defined on Ω_T, such that $U_i|_{\Gamma_D} > 0$, $i = 1,2$, for all $t \in (0,T)$, and X_0 is a given function defined on Ω, with $X_0 \geq 0$ for almost every (a.e.) $\boldsymbol{x} \in \Omega$. The above Dirichlet-Neumann boundary conditions represent the standard choice in semiconductor device modeling [30,31,27]. More general Robin-type boundary conditions are considered in [25], and will be discussed in the numerical experiments of Sect. 5.

Problem (1)-(3) is a system of non-linearly coupled partial differential equations for the scalar unknowns u_1, u_2 and X. Equations $(1)_2$, for $i = 1,2$, are advection-diffusion-reaction conservation laws analogous to those considered in [36,42,43] in the case of inorganic semiconductors, with convective velocities $\boldsymbol{v}_i$ depending on the electric field $\boldsymbol{E} = -\boldsymbol{\nabla}\varphi$ consistently determined by the solution of the Poisson equation $(1)_1$. Unlike the case considered in [36,42,43], the above system is coupled with a kinetic ordinary differential equation describing the time evolution of the variable X. In the application at hand, the variables u_i represent the concentrations of photogenerated electrons ($q_1 = -q$) and holes ($q_2 = +q$), while X is the concentration of geminate charge pairs. It is interesting to notice that the model (1)-(3) can be easily extended to cover the more general case of an electro-chemical system of N_{carr} charged carriers u_i interacting with M_{chem} chemical species X_j. This allows to

adopt the analytical and computational techniques developed in the present work to study other advanced photovoltaic devices for energy solar conversion, such as the dye-sensitized solar cells proposed in [19,18] and numerically investigated in [14], and will be the object of a forthcoming article.

According to conventional drift-diffusion theory (see, e.g., [27]), the convective velocities $\boldsymbol{v}_i$ are assumed to be proportional to the applied electric field

$$\boldsymbol{v}_1 = \mu_1 \boldsymbol{E}, \qquad \boldsymbol{v}_2 = -\mu_2 \boldsymbol{E}, \tag{4}$$

the coefficients μ_i being the electron and hole mobilities, described by the following Poole-Frenkel model [17,24], combined with a velocity saturation model

$$\mu_i = \left(\mu_{i,PF}^{-1} + \mu_{i,sat}^{-1}\right)^{-1} \qquad i = 1, 2, \tag{5}$$

where

$$\mu_{i,PF} = \mu_{i0} \exp\left(-\frac{\delta_i}{K_B T_{eff}} + \sqrt{|\boldsymbol{E}|}\left(\frac{\beta_i}{K_B T_{eff}} - \gamma_i\right)\right)$$

and

$$\mu_{i,sat} = \frac{v_{i,max}}{|\boldsymbol{E}|},$$

K_B denoting the Boltzmann constant. A discussion of physically consistent values for the model parameters δ_i, β_i, γ_i, T_{eff} and $v_{i,sat}$ is given along with the numerical results in Section 5. Moreover, as done also in [25,43], the Einstein relation between mobilities and diffusivities D_i is assumed to hold

$$D_i = V_{th} \mu_i \qquad i = 1, 2, \tag{6}$$

$V_{th} = K_B T/q$ denoting the thermal voltage corresponding to an absolute temperature T. Relation (6) will be conveniently exploited in the analysis of the existence of a solution of model (1)-(3) in the stationary case.

The specific form of the generation/recombination terms R_i, G_i, r and g is as follows:

$$\begin{cases} G_1 = G_2 = k_{diss}(|\boldsymbol{E}|)X, & \\ R_1 = \gamma u_2, & R_2 = \gamma u_1, \\ g = G + \gamma u_1 u_2, & r = (k_{diss}(|\boldsymbol{E}|) + k_{rec})X, \end{cases} \tag{7}$$

where the charge pairs recombination rate k_{rec} is a given constant, the photon generation rate G is a given function of $\boldsymbol{x}$ and t, the bimolecular recombination rate γ is of the Langevin form [33]

$$\gamma = \frac{q}{\varepsilon}(\mu_1 + \mu_2), \tag{8}$$

and the dissociation rate is [33]

$$k_{diss}(|\boldsymbol{E}|) = \frac{3\,\gamma}{4\pi a^3} \exp\left(-\frac{E_B}{K_B T}\right) \Phi(b(|\boldsymbol{E}|)), \tag{9}$$

a being the initial separation of the bound electron-hole $(e-h)$ pair, E_B the $e-h$ pair binding energy, $\Phi(x) = J_1(2\sqrt{-2x})/\sqrt{-2x} = 1+x+x^2/3+x^3/18+x^4/180+\cdots$ (where J_1 is the Bessel function of the first kind), and

$$b(|\boldsymbol{E}|) = \frac{q^3\,|\boldsymbol{E}|}{8\pi\varepsilon K_B^2 T^2}.$$

3 System Analysis of the Model

In this section, we deal with the analysis of the existence of a solution of system (1)-(3) in both stationary and transient regimes. From now on, as commonly done in the case of inorganic semiconductor device modeling, we indicate by n and p the concentrations of photogenerated electrons and holes, resp., (formerly denoted by u_1 and u_2). Moreover, we assume that the model parameters γ, k_{diss}, k_{rec} and G are all positive constant quantities in Ω_T. This allows us to express in an easy manner the dependent variable X as a function of n, p and of the input data G and X_0, in such a way that the resulting equivalent system of PDEs (in the reduced set of unknowns φ, n and p) can be written in the form of a two-carrier drift-diffusion (DD) model. In the stationary case, it is possible to apply the techniques of [31] to prove the existence of a solution of the problem, and it is expected that an analogous result can be obtained by properly adapting the invariant region theory proposed in [10,12] if the generation/recombination terms are as in (7)-(9). In the transient case, the extension to the present setting of available results for the DD model (see, e.g., [37,36,42,43] and the more recent work [44]) turns out to be a non-trivial matter, because of the presence of an integro-differential term at the right-hand side of the continuity equations for n and p. A first attempt of the present work to address the study of the transient problem in an OSC consists of approximating the above integro-differential term by the trapezoidal quadrature rule. This model reduction approach allows us, on the one hand, to use the techniques of [42,43] to prove the existence of a solution of the (approximate) differential system, and, on the other hand, to better highlight the role of exciton dynamics in determining the device turn-on time. In the case of one-dimensional mono-layer structures as those considered in the numerical experiments of Sect. 5, an alternative approach for the analysis of the existence of a solution in the transient regime of the full model (1)-(3) with (7)-(9), based on a temporal semi-discretization using the Backward Euler method as proposed in [11], is currently under investigation.

3.1 Notation

We let $H := W^{1,2}(\Omega)$ denote the usual (real) Sobolev space and let H_0 be the subspace of H defined by $H_0 = \{v \in H \mid v|_{\Gamma_D} = 0\}$. To study the time evolution of system (1)-(3), we also introduce the space $Y := L^2(0,T;H_0)$ of square integrable functions on $(0,T)$, with values in H_0.

3.2 Analysis in the Stationary Regime

Setting $\partial X/\partial t = 0$ in $(1)_3$, we can eliminate the dependent variable X in favor of n, p and of the input function G to obtain

$$X(\boldsymbol{x}) = \tau\left(G + \gamma p(\boldsymbol{x}) n(\boldsymbol{x})\right), \tag{10}$$

where $\tau := (k_{diss} + k_{rec})^{-1}$ is the time of response of the generation/recombination terms to light stimuli. Upon replacing (10) into the right-hand side of the continuity equations $(1)_2$, system (1)–(2) in stationary conditions assumes the following form:

$$\begin{cases} -\mathrm{div}(\varepsilon \boldsymbol{\nabla}\varphi) = q(p-n), \\ -\mathrm{div}\boldsymbol{J}_n \quad = \tau\left(k_{diss}\, G - \gamma\, k_{rec}\, pn\right), \\ \boldsymbol{J}_n \quad = D_n \boldsymbol{\nabla} n - \mu_n n \boldsymbol{\nabla}\varphi, \\ -\mathrm{div}\boldsymbol{J}_p \quad = \tau\left(k_{diss}\, G - \gamma\, k_{rec}\, pn\right), \\ \boldsymbol{J}_p \quad = D_p \boldsymbol{\nabla} p + \mu_p p \boldsymbol{\nabla}\varphi. \end{cases} \tag{11}$$

The analysis of the existence of a solution of (11) simplifies considerably by exploiting the Einstein relation (6) to write the two flux densities as

$$\begin{cases} \boldsymbol{J}_n = D_n\, n_r\ \mathrm{e}^{\varphi/V_{th}}\, \boldsymbol{\nabla} u, \\ \boldsymbol{J}_p = D_p\, n_r\ \mathrm{e}^{-\varphi/V_{th}}\, \boldsymbol{\nabla} v, \end{cases} \tag{12}$$

where the new (adimensional) dependent variables u and v are related to the carrier densities n and p by the Maxwell–Boltzmann statistics

$$n = n_r\, u\, \mathrm{e}^{\varphi/V_{th}}, \qquad p = n_r\, v\, \mathrm{e}^{-\varphi/V_{th}}, \tag{13}$$

$n_r > 0$ being a yet unspecified reference carrier concentration. From (13), we see that u and v must be positive in Ω since n and p represent "physical" concentrations. Replacing (12) and (13) into (11), and choosing n_r in such a way that $(\gamma k_{rec} n_r^2)/(k_{diss} G) = 1$, leads to study, for $\boldsymbol{x} \in \Omega$, the following non-linear elliptic partial differential system in the unknowns φ, u and v:

$$\begin{cases} -\mathrm{div}(\varepsilon \boldsymbol{\nabla} \varphi) & = q\, n_r (u\, \mathrm{e}^{\varphi/V_{th}} - v\, \mathrm{e}^{-\varphi/V_{th}}), \\ -\mathrm{div}(D_n\ \mathrm{e}^{\varphi/V_{th}}\, \boldsymbol{\nabla} u) & = \dfrac{\tau k_{diss} G}{n_r}(1 - uv), \\ -\mathrm{div}(D_p\ \mathrm{e}^{-\varphi/V_{th}}\, \boldsymbol{\nabla} v) & = \dfrac{\tau k_{diss} G}{n_r}(1 - uv), \end{cases} \tag{14}$$

supplied with the boundary conditions

$$\begin{cases} \varphi = \Psi_D, \quad u = (n_D/n_r)\ \mathrm{e}^{-\Psi_D/V_{th}}, \quad v = (p_D/n_r)\ \mathrm{e}^{\Psi_D/V_{th}} & \text{on } \Gamma_D, \\ \boldsymbol{J}_n \cdot \boldsymbol{\nu} = \boldsymbol{J}_p \cdot \boldsymbol{\nu} = \boldsymbol{\nabla} \varphi \cdot \boldsymbol{\nu} = 0 & \text{on } \Gamma_N, \end{cases} \tag{15}$$

where $(\Psi_D, n_D, p_D) \in (L^\infty(\Gamma_D))^3$, $n_D > 0$ and $p_D > 0$ being the Dirichlet boundary data for n and p, respectively. Let us set

$$u_D := (n_D/n_r)\ \mathrm{e}^{-\Psi_D/V_{th}} \equiv \mathrm{e}^{-\varphi_{nD}/V_{th}}, \qquad v_D := (p_D/n_r)\ \mathrm{e}^{\Psi_D/V_{th}} \equiv \mathrm{e}^{\varphi_{pD}/V_{th}},$$

with $u_D > 0$, $v_D > 0$, and where

$$\varphi_{nD} := \Psi_D - V_{th} \ln(n_D/n_r), \qquad \varphi_{pD} := \Psi_D + V_{th} \ln(p_D/n_r).$$

Then, we can see that there exists $\Psi^+ \geq 0$ such that

$$\mathrm{e}^{-\Psi^+/V_{th}} \leq u_D(\boldsymbol{x}),\ v_D(\boldsymbol{x}) \leq \mathrm{e}^{\Psi^+/V_{th}} \qquad \text{for a.e. } \boldsymbol{x} \in \Gamma_D, \tag{16}$$

where

$$\Psi^+ := \max\left\{ \max(\sup_{\Gamma_D}(-\varphi_{nD}), \sup_{\Gamma_D}(\varphi_{pD})), -\min(\inf_{\Gamma_D}(-\varphi_{nD}), \inf_{\Gamma_D}(\varphi_{pD})) \right\}.$$

Following the guideline of [31], Sect.3.3, we can prove the result below.

Theorem 1 (Existence of a solution in stationary regime) *Let u_D and v_D satisfy* (16)*. Then, system* (14)–(15) *admits a weak solution $(\varphi^*, u^*, v^*) \in (H^1(\Omega) \cap L^\infty(\Omega))^3$ which satisfies the L^∞-estimate*

$$\begin{aligned} &\mathrm{e}^{-\Psi^+/V_{th}} \leq u^*(\boldsymbol{x}),\ v^*(\boldsymbol{x}) \leq \mathrm{e}^{\Psi^+/V_{th}} && \text{for a.e. } \boldsymbol{x} \in \Omega, \\ &\min\left(\inf_{\Gamma_D} \Psi_D,\ -\Psi^+\right) \leq \varphi^*(\boldsymbol{x}) \leq \max\left(\sup_{\Gamma_D} \Psi_D,\ \Psi^+\right) && \text{for a.e. } \boldsymbol{x} \in \Omega. \end{aligned} \tag{17}$$

Going back to the original variables n and p through (13), we immediately conclude that system (11) admits a solution $(\varphi^*, n^*, p^*) \in (H^1(\Omega) \cap L^\infty(\Omega))^3$ which satisfies the L^∞-estimate

$$n_r \ \mathrm{e}^{-\widehat{\Psi}^+/V_{th}} \leq n^*(\boldsymbol{x}),\ p^*(\boldsymbol{x}) \leq n_r \ \mathrm{e}^{\widehat{\Psi}^+/V_{th}} \qquad \text{for a.e. } \boldsymbol{x} \in \Omega, \tag{18}$$

where $\widehat{\Psi}^+ := \sup_{\Gamma_D} |\Psi_D| + \Psi^+$.

3.3 Analysis in Transient Regime

Analogously to what we have done in Sect. 3.2 in the stationary case, we can use $(1)_3$ to eliminate the dependent variable X in favor of n, p and of the input functions G and X_0, to obtain

$$X(\boldsymbol{x},t) = \xi(\boldsymbol{x},t) + \gamma \int_0^t p\ n\, \mathrm{e}^{-(t-s)/\tau}\ ds, \tag{19}$$

where $\xi(\boldsymbol{x},t) := X_0(\boldsymbol{x})\, \mathrm{e}^{-t/\tau} + \tau\ G(1 - \mathrm{e}^{-t/\tau})$. Upon replacing (19) into the right-hand side of $(1)_2$, we can write the continuity equations for the photogenerated electrons and holes in the following form:

$$\begin{cases} \dfrac{\partial n}{\partial t} - \mathrm{div}\boldsymbol{J}_n = f(\boldsymbol{x},t) - \gamma\, \tau\, p\, n \left(k_{rec} + k_{diss}\, \mathrm{e}^{-t/\tau}\right) + \ I_\lambda(t) \\ \dfrac{\partial p}{\partial t} - \mathrm{div}\boldsymbol{J}_p = f(\boldsymbol{x},t) - \gamma\, \tau\, p\, n \left(k_{rec} + k_{diss}\, \mathrm{e}^{-t/\tau}\right) + \ I_\lambda(t), \end{cases} \tag{20}$$

where $f(\boldsymbol{x},t) := k_{diss}\xi(\boldsymbol{x},t)$ and

$$I_\lambda(t) := \gamma\, k_{diss} \int_0^t [\lambda(s) - \lambda(t)]\, \mathrm{e}^{-(t-s)/\tau}\ ds, \tag{21}$$

with $\lambda(t) := p(\cdot,t)\ n(\cdot,t)$. The three contributions at the right-hand sides of $(20)_1$ and $(20)_2$ have an interesting physical meaning. The first two contributions (one strictly positive, the other strictly negative) account for the generation and recombination mechanisms occurring instantaneously (i.e., at time t), while the third contribution (that does not have *a-priori* a definite sign) is a convolution term, which makes the dependence of the current on the electron and hole densities to be non-local in time but with a "memory window" of size proportional to τ, acting in a similar manner to non–linear viscosity mechanisms in viscoelastic models [39]. The presence of the convolution term I_λ makes the form of the production terms in the OSC continuity equations significantly different from those in the classical DD continuity equations for inorganic semiconductor device modeling [38,30,31,27]. This fact has two

important consequences, one of physical nature, the other of mathematical nature. On the one hand, devising a simple physical picture to interpret the photocurrent transient in an OSC is far from immediate, thus clearly justifying the continuous increase in the use of simulation tools (see, e.g.., [8,25] and the references cited therein). On the other hand, extending to the case of OSCs the existence results available in the case of the transient DD model (see, e.g., [36,42,43] and [1,44]) is an absolutely non-trivial task.

The above considerations suggest to operate a consistent simplification of the model equations (20)–(21) through a suitable approximation of $I_\lambda(t)$. With this aim, we assume that the dependent variables n and p are sufficiently smooth functions of $\boldsymbol{x}$ and t, and we let

$$g_\tau(s;t) := [\lambda(s) - \lambda(t)]\, \mathrm{e}^{-(t-s)/\tau},$$

from which we have $g_\tau(t;t) = 0$ for all t. Then, replacing $I_\lambda(t)$ with its quadrature given by the trapezoidal rule, yields

$$I_\lambda(t) \simeq \widetilde{I}_\lambda(t) = \gamma\, k_{diss} \frac{t}{2} \left[g_\tau(0;t) + g_\tau(t;t) \right] = \gamma\, k_{diss}\, \frac{t}{2}\, \mathrm{e}^{-t/\tau} \left[\lambda(0) - \lambda(t) \right], \tag{22}$$

where the positive term proportional to $\lambda(0)$ can be regarded as a contribution to the free carrier generation process and the negative term proportional to $-\lambda(t)$ can be regarded as a contribution to the free carrier recombination process. The approximate model to describe photocurrent transients in an OSC is then obtained replacing the convolution term $I_\lambda(t)$ in (20) with $\widetilde{I}_\lambda(t)$, and reads:

$$\begin{cases} -\mathrm{div}(\varepsilon \boldsymbol{\nabla} \varphi) &= q(p-n), \\ \dfrac{\partial n}{\partial t} - \mathrm{div} \boldsymbol{J}_n &= G_n(\boldsymbol{x},t,n,p) - R_n(\boldsymbol{x},t,n,p) n, \\ \boldsymbol{J}_n &= D_n \boldsymbol{\nabla} n - \mu_n n \boldsymbol{\nabla} \varphi, \\ \dfrac{\partial p}{\partial t} - \mathrm{div} \boldsymbol{J}_p &= G_p(\boldsymbol{x},t,n,p) - R_p(\boldsymbol{x},t,n,p) p, \\ \boldsymbol{J}_p &= D_p \boldsymbol{\nabla} p + \mu_p p \boldsymbol{\nabla} \varphi, \end{cases} \tag{23}$$

where the modified generation/recombination mechanisms are defined as

$$\begin{cases} G_n(\boldsymbol{x},t,n,p) &= G_p(\boldsymbol{x},t,n,p) = f(\boldsymbol{x},t) + \gamma\, k_{diss} \dfrac{t}{2}\, \mathrm{e}^{-t/\tau}\, n(\cdot,0)\, p(\cdot,0) \\ \\ R_n(\boldsymbol{x},t,n,p) n = R_p(\boldsymbol{x},t,n,p) p &= \gamma \left[\tau (k_{rec} + k_{diss}\, \mathrm{e}^{-t/\tau}) + k_{diss} \dfrac{t}{2}\, \mathrm{e}^{-t/\tau} \right] np. \end{cases} \tag{24}$$

Having derived a new, simplified, model, it is natural to ask to which extent the novel formulation is capable to describe correctly the main features of the performance of an OSC. With this aim, we first investigate the quality of the approximation provided by $\widetilde{I}_\lambda(t)$, and then we address the analysis of the existence of a solution for the approximate model.

The quadrature error $E(t) := I_\lambda(t) - \widetilde{I}_\lambda(t)$ associated with the use of the trapezoidal rule in (22) is given by the following relation [34]

$$\begin{aligned} E(t) &= -\frac{t^3}{12}\left(\lambda''(\eta)e^{-(t-\eta)/\tau} + 1/\tau^2 g_\tau(\eta;t)\right) \\ &= -\frac{t^3}{12}e^{-t/\tau}\left(\lambda''(\eta) + 1/\tau^2(\lambda(\eta)-\lambda(t))e^{s/\tau})\right), \end{aligned} \tag{25}$$

where $\eta \in (0,t)$. Eq. (25) shows that $E(t)$ becomes negligible as $t \to 0$ or $t \to +\infty$. This means that the predicted (computed) stationary current is independent of the use of (22) or the exact expression $I_\lambda(t)$ in (20), as numerically verified by the simulations discussed in Sect. 5.1. However, for a finite value of time t, the discrepancy between the exact convolution term and its approximation may be non-negligible. A reasonable estimate of the error would require a knowledge on the temporal behavior of the photogenerated carrier densities n and p as a function of time. This knowledge not being available, we can still gain some information on the quadrature error by an analogy with the approximation of the recombination/generation term that is usually carried out in the study of currents in a $p-n$ junction in the inorganic case (see [40]). This analogy suggests that the value of $E(t)$ during the photocurrent transient (i.e., for t sufficiently far from 0 but also sufficiently far from stationary conditions) might become significant if the OSC is operating under high injection conditions, or, equivalently, high current level conditions. Again, this latter statement is numerically verified by the simulations discussed in Sect. 5.1.

We conclude the analysis of the simplified model for an OSC proving the existence of a solution of system (23)-(24) subject to the initial/boundary conditions (3). For this, we refer to [42,43], and check whether the problem coefficients D_ν, $\boldsymbol{v}_\nu$ and R_ν, for $\nu = \{n,p\}$, satisfy all of the assumptions (Ei)–(Eiv) of [42], p. 296 and (H1)–(H4) of [43], p. 1202. It is immediate to see that the functions R_n and R_p are positive for $p > 0$ and $n > 0$ and satisfy locally Lipschitz conditions, with a Lipschitz constant which is uniform in time and equal to 2γ. As a matter of fact, for R_n we have, for all n', p', n'', p'' and for all $\boldsymbol{x}$ and t

$$\begin{aligned} |R_n(\boldsymbol{x},t,n',p') - R_n(\boldsymbol{x},t,n'',p'')| &\le \gamma\ \left(\tau(k_{rec}+k_{diss}) + \tau k_{diss}\right)|p'-p''| \\ &\le 2\gamma|p'-p''|, \end{aligned}$$

and the same estimate holds for R_p provided to exchange $|p'-p''|$ with $|n'-n''|$.

Moreover, the choice of the mobility model (5) ensures that there exist positive constants D^{min}, D^{max} and v^{max} such that

$$0 < D^{min} \leq D_n(\boldsymbol{x}, t), D_p(\boldsymbol{x}, t) \leq D^{max} \qquad \text{for a.e. } (\boldsymbol{x}, t) \in \Omega_T,$$

and

$$|\boldsymbol{v}_n(\boldsymbol{x}, t)|, |\boldsymbol{v}_p(\boldsymbol{x}, t)| \leq v^{max} \qquad \text{for a.e. } (\boldsymbol{x}, t) \in \Omega_T.$$

The above properties of the problem coefficients ensure that the required assumptions of [42] and [43] are verified, so that we can prove the result below.

Theorem 2 (Existence of a solution in the transient regime) *Let the initial data $\boldsymbol{U}$ and X_0, and the function Ψ be such that $\boldsymbol{U} \in H^1(\Omega_T) \cap L^\infty(\Omega_T)$, with $\boldsymbol{U} > \boldsymbol{0}$, $X_0 \in L^\infty(\Omega)$ with $X_0 \geq 0$, and $\Psi \in H^1(\Omega_T) \cap L^\infty(\Omega_T)$. Then, setting $\boldsymbol{u} = [n, p]^T$, system (23)-(24), supplied with the initial/boundary conditions (3), admits a weak solution $(\varphi, \boldsymbol{u})$ such that:*

(1) $\boldsymbol{u} > \boldsymbol{0}$ *a.e. in* Ω_T*;*
(2) $\boldsymbol{u}(\boldsymbol{x}, 0) = \boldsymbol{U}(\boldsymbol{x}, 0)$ *and* $\boldsymbol{u} - \boldsymbol{U} \in L^2(0, T; H_0)$*;*
(3) $\boldsymbol{u} \in C(0, T; L^2(\Omega)) \cap L^\infty(\Omega_T)$*;*
(4) $\dfrac{\partial \boldsymbol{u}}{\partial t} \in L^2(0, T; H_0')$*;*
(5) $\varphi - \Psi \in L^2(0, T; H_0)$ *with* $\varphi \in L^\infty(\Omega_T)$*;*

and satisfying

$$\begin{cases} \displaystyle\int_\Omega \varepsilon \boldsymbol{\nabla}\varphi(t) \cdot \boldsymbol{\nabla}\eta = \int_\Omega \left(\sum_{i=1}^{2} q_i u_i(t) \right) \eta & \text{for a.e. } t \in [0, T], \\ \displaystyle\int_{\Omega_T} \frac{\partial u_i}{\partial t} \rho_i + \int_{\Omega_T} \boldsymbol{J}_i \cdot \boldsymbol{\nabla}\rho_i & \\ \displaystyle + \int_{\Omega_T} R_i(\boldsymbol{x}, t, \boldsymbol{u}) u_i \rho_i = \int_{\Omega_T} G_i(\boldsymbol{x}, t, \boldsymbol{u}) \rho_i & i = 1, 2, \end{cases} \tag{26}$$

for all $\eta \in H_0$ and $\boldsymbol{\rho} = [\rho_1, \rho_2]^T \in Y$.

Using the representation formula (19) and the regularity of X_0, n and p, we have that

$$X, \frac{\partial X}{\partial t} \in C(0, T; L^2(\Omega)) \cap L^\infty(\Omega_T)$$

with $X(\boldsymbol{x}, t) > 0$ for all $t > 0$ and for a.e. $\boldsymbol{x} \in \Omega$.

4 Numerical Discretization

In this section, we illustrate the numerical techniques for the simulation of the full model (1)–(3), as the same approach can be used, with slight modifications, to treat the reduced approximate model (23)–(24). In designing

the algorithm presented here, our aim is twofold: on the one hand, it seems natural to try to adapt methods that are known to work efficiently and reliably for transient simulation of inorganic semiconductor devices (see, *e.g.*, [38] Chapt. 6, Sect. 4); on the other hand, as the emphasis of the present paper is on accurately estimating photocurrent transient times, it is necessary to apply advanced time-step control techniques [3,23]. To this end, our chosen approach is based on Rothe's method (also known as method of horizontal lines) which consists of three main steps: first, the time dependent problem is transformed into a sequence of stationary differential problems by approximating the time derivatives by a suitable difference formula; then, the resulting nonlinear problems are linearized by an appropriate functional iteration scheme; and, finally, the linear differential problems obtained are solved numerically using a Galerkin–Finite Element Method (G–FEM) for the spatial discretization. Sects. 4.1, 4.2 and 4.3 below discuss in more detail each of these steps; it is worth noting that, with minor modifications, the linearization techniques of Sect. 4.2 can also be applied to treat the stationary model (11).

4.1 Time Discretization

To transform the time dependent problem (1)–(3) into a sequence of stationary problems, we replace the partial time derivative with a suitable finite difference approximation, specifically, the Backward Differencing Formulas (BDF) of order $m \leq 5$ (see, *e.g.*, [3], Sect. 10.1.2). To describe the resulting stationary problem, let $0 = t_0 < \ldots < t_{K-1} < t_K < T$ be a strictly increasing, not necessarily uniformly spaced, finite sequence of time levels and assume the quantities $u_1 = n$, $u_2 = p$, X and φ to be known functions of $\boldsymbol{x}$ for every t_k, $k = 0 \ldots K-1$. Then we can then rewrite (1) as:

$$\begin{cases} -\mathrm{div}(\varepsilon \boldsymbol{\nabla} \varphi_K) + q\,(n_K - p_K) & = 0 \\ \displaystyle\sum_{k=0}^{m} \theta_k n_{K-k} - \mathrm{div}\boldsymbol{J}_n(n_K; \boldsymbol{\nabla}\varphi_K) - U_K & = 0 \\ \displaystyle\sum_{k=0}^{m} \theta_k p_{K-k} - \mathrm{div}\boldsymbol{J}_p(p_K; \boldsymbol{\nabla}\varphi_K) - U_K & = 0 \\ \displaystyle\sum_{k=0}^{m} \theta_k X_{K-k} - W_K & = 0, \end{cases} \tag{27}$$

where $f_k = f(\boldsymbol{x}, t_k)$ for any generic function $f = f(\boldsymbol{x}, t)$, and

$$
\begin{aligned}
U_K &:= U(\boldsymbol{\nabla}\varphi_K, n_K, p_K, X_K, t_K) \\
&= G_n(\boldsymbol{\nabla}\varphi_K, n_K, p_K, X_K, t_K) - R_n(\boldsymbol{\nabla}\varphi_K, n_K, p_K, X_K, t_K)\ n_K \\
&= G_p(\boldsymbol{\nabla}\varphi_K, n_K, p_K, X_K, t_K) - R_p(\boldsymbol{\nabla}\varphi_K, n_K, p_K, X_K, t_K)\ p_K,
\end{aligned}
$$

$$
\begin{aligned}
W_K &:= W(\boldsymbol{\nabla}\varphi_K, n_K, p_K, X_K, t_K) \\
&= g(\boldsymbol{\nabla}\varphi_K, n_K, p_K, X_K, t_K) - r(\boldsymbol{\nabla}\varphi_K, n_K, p_K, X_K, t_K).
\end{aligned}
$$

System (27), together with the constitutive relations for the fluxes given in (2) and the set of boundary conditions (3), constitutes a system of non-linear elliptic differential equations ($(27)_{1-3}$) coupled to an algebraic constraint equation ($(27)_4$). In our implementation, the selection of the next time level t_K and of the formula's order m, as well as the computation of the corresponding coefficients $\theta_k, k = 0, \ldots, m$, is performed adaptively to minimize the time discretization error while minimizing the total number of time steps via the DAE solver software library DASPK [7,41]. Notice that, if $m = 1$, we have $\theta_0 = -\theta_1 = \frac{1}{t_K - t_{K-1}}$, $\theta_k = 0,\ k > 1$, and the temporal semi-discretization of system (1)–(3) coincides with the Backward Euler method.

4.2 Linearization

To ease the notation, throughout this section the subscripts denoting the current time level will be dropped. Let $\boldsymbol{y} := [\varphi,\ n,\ p,\ X]^T$ denote the vector of dependent variables and let $\mathbf{0}$ denote the null vector in $\mathbb{R}^4$. Then, the non-linear system (27) can be written in compact form as

$$
\mathbf{F}(\boldsymbol{y}) = \mathbf{0}, \qquad \text{with} \qquad \mathbf{F}(\boldsymbol{y}) = \left\{ \begin{array}{l} f_\varphi(\varphi, n, p) \\ f_n(\varphi, n, p, X) \\ f_p(\varphi, n, p, X) \\ f_X(\varphi, n, p, X) \end{array} \right\}. \tag{28}
$$

The adopted functional iteration technique for the linearization and successive solution of problem (27) is the Newton-Raphson method. One step of this scheme can be written as

$$
\left[\begin{array}{cccc} \partial_\varphi(f_\varphi) & \partial_n(f_\varphi) & \partial_p(f_\varphi) & 0 \\ \partial_\varphi(f_n) & \partial_n(f_n) & \partial_p(f_n) & \partial_X(f_n) \\ \partial_\varphi(f_p) & \partial_n(f_p) & \partial_p(f_p) & \partial_X(f_p) \\ \partial_\varphi(f_X) & \partial_n(f_X) & \partial_p(f_X) & \partial_X(f_X) \end{array} \right]_{(\varphi,n,p,X)} \left[\begin{array}{c} \Delta\varphi \\ \Delta n \\ \Delta p \\ \Delta X \end{array} \right] = \left[\begin{array}{c} -f_\varphi(\varphi, n, p) \\ -f_n(\varphi, n, p, X) \\ -f_p(\varphi, n, p, X) \\ -f_X(\varphi, n, p, X) \end{array} \right] \tag{29}
$$

where $\partial_a(f)$ denotes the Frechét derivative of the non-linear operator f with respect to the function a. More concisely, we can express (29) in matrix form as

$$\mathbf{J}(\boldsymbol{y})\ \Delta\boldsymbol{y} = -\mathbf{F}(\boldsymbol{y}),$$

where $\mathbf{J}$ is the Jacobian matrix and $\Delta\boldsymbol{y} := [\Delta\varphi,\ \Delta n,\ \Delta p,\ \Delta X]^T$ is the unknown increment vector. The exact computation of all the derivatives in the Jacobian on the left hand side in (29) can become quite complicated if the full model for all the coefficients (most notably the electric field dependence of k_{diss}, μ_n and μ_p) is taken into account. Moreover, this would require non-trivial modifications to the solver code whenever a new coefficient model is to be implemented. One alternative could be to employ a staggered solution algorithm, often referred to as Gummel-type approach in the semiconductor simulation context [21,12]. The decoupled approach is well known to be more robust as compared to the fully coupled Newton approach (29) with respect to the choice the initial guess and also less memory consuming. As in this particular study we can rely on the knowledge of the system variables at previous time levels to construct a reasonable initial guess and as we are dealing with an intrinsically one-dimensional problem (see Sect. 5), memory occupation is not likely to be a stringent constraint, so that we adopt a quasi-Newton method where, rather than the exact Jacobian $\mathbf{J}(\boldsymbol{y})$ we use an approximation $\widetilde{\mathbf{J}}(\boldsymbol{y})$ in which the dependence of the mobilities, of the diffusion coefficients and of the dissociation coefficient on the electric field is neglected. This approach has the further advantage of facilitating the use of a standard software library like DASPK for advancing in time.

4.3 Spatial Discretization and Balancing of the Linear System

Once the linearization described in the previous section is applied, the resulting linear system of PDEs is numerically approximated by means of a suitable G–FEM. Precisely, to avoid instabilities and spurious oscillations that may arise when the drift terms become dominant, we employ an exponential fitting finite element discretization [5,16,46,29]. This formulation provides a natural multi-dimensional extension of the classical Scharfetter-Gummel difference scheme [35,6] and ensures, when applied to a carrier continuity equation in the DD model, that the computed carrier concentration is strictly positive under the condition that the triangulation of the domain $\overline{\Omega}$ is of Delaunay type. It is important to notice that, when implementing on the computer the above described procedure, the different physical nature of the unknowns of the system and their wide range of variation may lead to badly scaled and therefore ill-conditioned linear algebraic problems, which in turn can negatively affect the accuracy and efficiency of the algorithm. To work around this issue, we introduce two sets of scaling coefficients, denoted $\{\sigma_\varphi,\ \sigma_n,\ \sigma_p,\ \sigma_X\}$

and $\{\bar{\varphi},\ \bar{n},\ \bar{p},\ \bar{X}\}$, and restate problem (28) as

$$\begin{cases} \dfrac{1}{\sigma_\varphi} f_\varphi(\bar{\varphi}\hat{\varphi}, \bar{n}\hat{n}, \bar{p}\hat{p}) = 0 \\ \dfrac{1}{\sigma_n} f_n(\bar{\varphi}\hat{\varphi}, \bar{n}\hat{n}, \bar{p}\hat{p}, \bar{X}\hat{X}) = 0 \\ \dfrac{1}{\sigma_p} f_p(\bar{\varphi}\hat{\varphi}, \bar{n}\hat{n}, \bar{p}\hat{p}, \bar{X}\hat{X}) = 0 \\ \dfrac{1}{\sigma_X} f_X(\bar{\varphi}\hat{\varphi}, \bar{n}\hat{n}, \bar{p}\hat{p}, \bar{X}\hat{X}) = 0, \end{cases} \tag{30}$$

where $\hat{\varphi} := \varphi/\bar{\varphi}$, $\hat{n} := n/\bar{n}$, $\hat{p} := p/\bar{p}$ and $\hat{X} := X/\bar{X}$. Solving (30) for the scaled dependent variables $[\hat{\varphi},\ \hat{n},\ \hat{p},\ \hat{X}]^T$ corresponds to solving a system equivalent to (29) where the rows of the Jacobian $\mathbf{J}$ and of the residual $\mathbf{F}$ are multiplied by the factors $\{1/\sigma_\varphi,\ 1/\sigma_n,\ 1/\sigma_p,\ 1/\sigma_X\}$ while the columns of $\mathbf{J}$ are multiplied by the factors $\{\bar{\varphi},\ \bar{n},\ \bar{p},\ \bar{X}\}$. Computational experience reveals that a proper choice of the scaling coefficients might have a strong impact on the performance of the algorithm. For example, to obtain the results of Fig. 7 a suitable choice was found to be that of setting $\sigma_\varphi = 1,\ \sigma_n = \sigma_p, = 10^3,\ \sigma_X = 10^2$ and $\bar{\varphi} = 1,\ \bar{n} = \bar{p}, = 10^{22},\ \bar{X} = 10^{19}$ while values differing by more than one order of magnitude from such choice were found to hinder the ability of the DAE solver to reach convergence.

5 Numerical Results

In this section, we carry out a thorough validation of the models and numerical techniques discussed and analyzed in the previous sections of the article. Given the intrinsically one-dimensional structure of BHJ cells, we assume henceforth that the computational domain is the interval $\Omega = [0,\ L_{OSC}]$. To allow an immediate comparison with [25], we set $L_{OSC} = 70nm$, $T = 300\ K$ and $E_B = 0.5\ eV$, while the relative permittivity constant is $\varepsilon_r = 4$ and the applied voltage is $\Delta V := \Psi_D(0) - \Psi_D(L_{OSC}) = 0.5\ V$.

5.1 The Case of Constant Problem Coefficients

In this section, the positive constant quantities k_{diss} is computed by replacing the spatially varying electric field E with its constant approximation $< E >:= -\Delta V/L_{OSC}$. Electron and hole mobilities are given constant values and, as a result of (8), also the bimolecular recombination rate is constant. In all subsequent graphical results, the dotted line refers to the solution computed

with the full model (19)-(20)-(21) while the solid line refers to the simplified approximate model (23)-(24).

Figures 1-2-3 refer to a device under low light intensity conditions and show the impact on the turn-on transient time of the value of the mobilities, of the geminate pair dissociation rate and of the recombination rate, respectively.

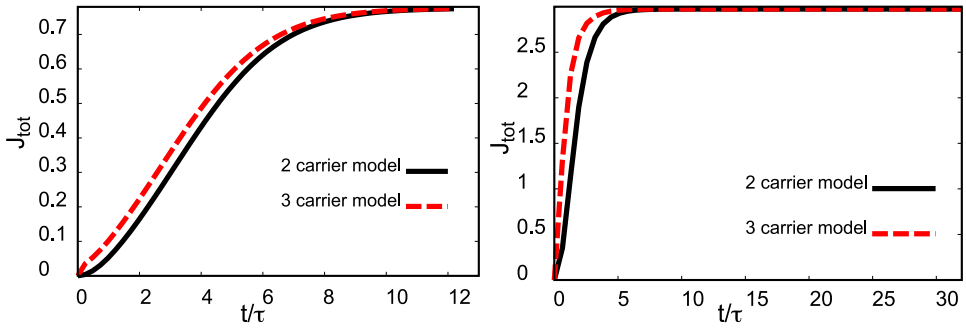

(a) Low mobilities: $\mu_n = \mu_p = 2 \times 10^{-9} m^2 V^{-1} s^{-1}$ (b) High mobilities: $\mu_n = \mu_p = 2 \times 10^{-8} m^2 V^{-1} s^{-1}$

Figure 1. Photocurrent transient at low light intensity: effect of mobility on rise time.

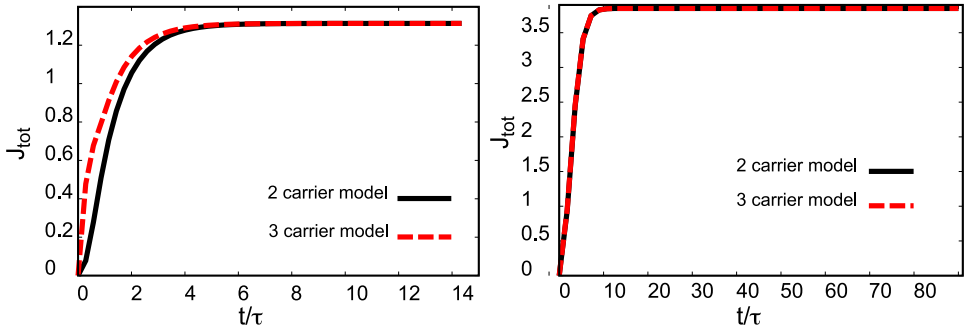

(a) $k_{diss} = 4.4 \times 10^5 s^{-1}$ (b) $k_{diss} = 8 \times 10^6 s^{-1}$

Figure 2. Photocurrent transient at low light intensity: effect of dissociation rate on rise time.

One may observe that, while at low intensity a change of one order of magnitude in the value of the mobility produces an almost equal change in the transient time, at high light intensity a similar change in the mobility has an almost negligible impact. In this latter regime, variations in the dissociation rate k_{diss} and, more notably the recombination rate k_{rec}, produce a more dramatic effect.

The analysis of the above results clearly shows that, even in the simple case of constant model coefficients, it is absolutely non-trivial to relate the transient

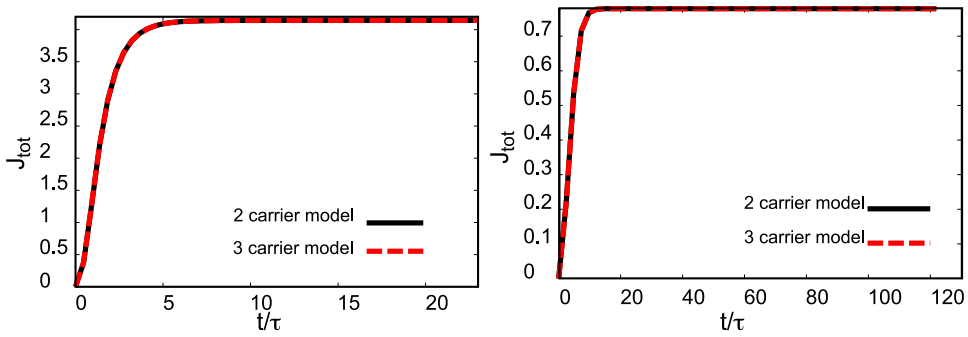

(a) $k_{rec} = 10^5 s^{-1}$ (b) $k_{rec} = 10^7 s^{-1}$

Figure 3. Photocurrent transient at low light intensity: effect of geminate pair recombination rate on rise time.

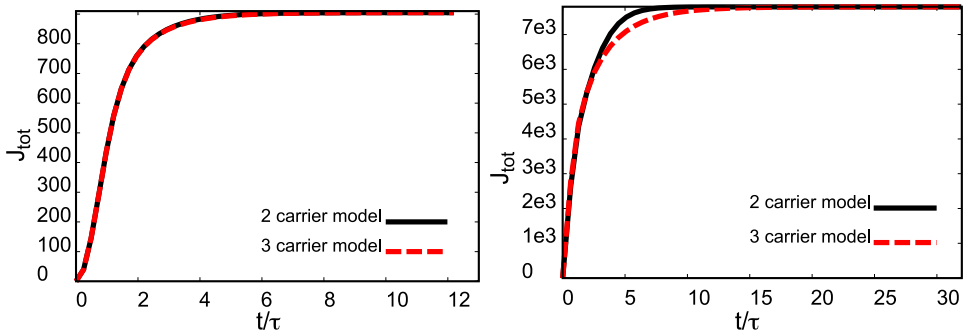

(a) Low mobilities: $\mu_n = \mu_p = 2 \times 10^{-9} m^2 V^{-1} s^{-1}$ (b) High mobilities: $\mu_n = \mu_p = 2 \times 10^{-8} m^2 V^{-1} s^{-1}$

Figure 4. Photocurrent transient at high light intensity: effect of mobility on rise time.

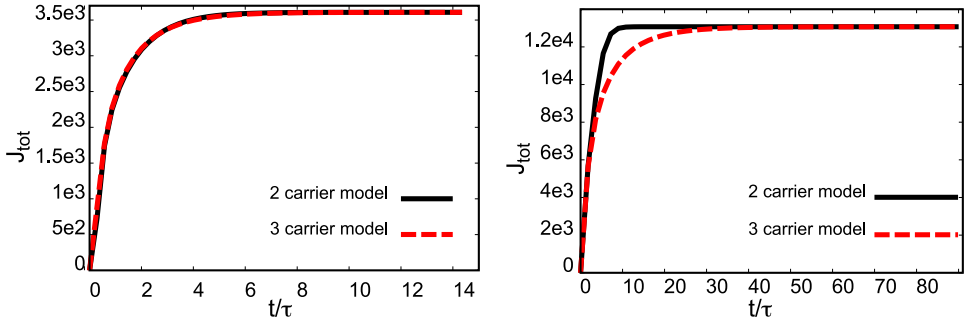

(a) $k_{diss} = 4.4 \times 10^5 s^{-1}$ (b) $k_{diss} = 8 \times 10^6 s^{-1}$

Figure 5. Photocurrent transient at high light intensity: effect of dissociation rate on rise time.

behavior of the device to a single model parameter, because of the strongly non-linear interplay of the several occurring physical phenomena.

As for the comparison of the simplified model (23)-(24) with respect to the full model (19)-(20)-(21) we observe that, as shown by the analysis of Sect. 3.3, the steady-state currents predicted by the two models always agree perfectly.

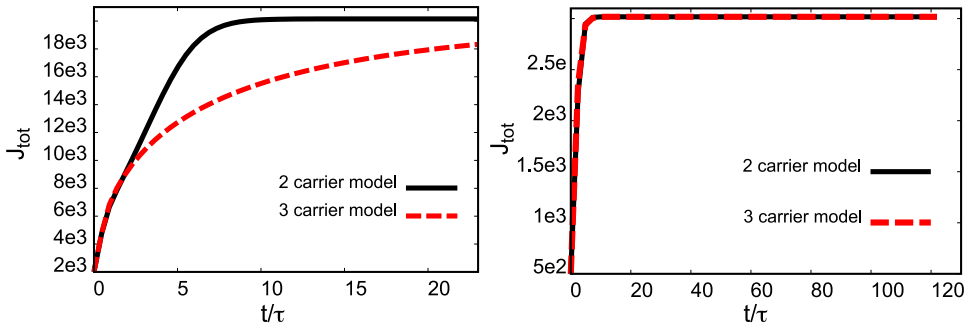

(a) $k_{rec} = 10^5 s^{-1}$ (b) $k_{rec} = 10^7 s^{-1}$

Figure 6. Photocurrent transient at high light intensity: effect of geminate pair recombination rate on rise time.

As for the prediction of the transient duration, the two models are in very good agreement except for the case of a device with high generation efficiency (i.e., a low value of k_{rec}) under high light intensity (cf. Fig. 6(a)), as anticipated in Sect. 3.3. This trend is confirmed by several other numerical experiments, not reported here, which seem to clearly indicate that the discrepancy between the model with exact evaluation of the convolution term $I_\lambda(t)$ and its approximate counterpart tends to occur in the high photocurrent regime.

5.2 The Case of Varying Problem Coefficients

In this section we compare the results of simulations performed by our code to that of [25]. With this aim, instead of the simple Dirichlet boundary conditions considered in this article, we have employed the more involved current injection model of [9]. Figure 7 shows the time evolution of the electron density

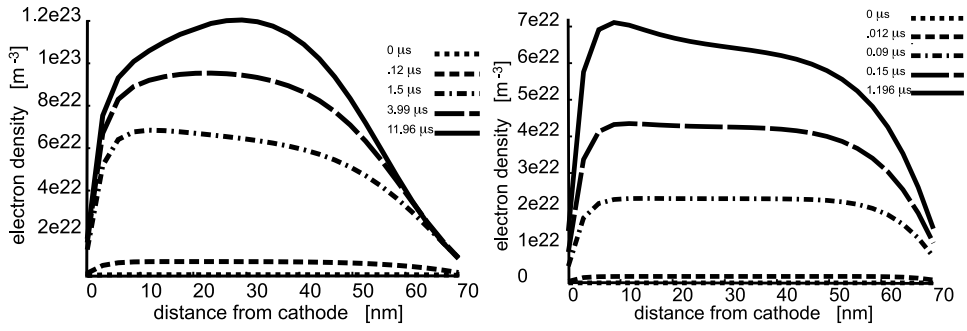

(a) $k_{rec} = 10^5 s^{-1}$ (b) $k_{rec} = 10^7 s^{-1}$

Figure 7. Time evolution of the electron distribution at high intensity with (a) high charge generation efficiency and (b) low charge generation efficiency.

in the device under strong illumination conditions ($G = 4.3 \cdot 10^{30}\ m^{-3}s^{-1}$). Hole density is not shown in the figures but, due to the choice of equal mobilities, it is the exact mirror image of the electron density. Notice that, for this

particular application, the carrier densities at a given point in the device are non-decreasing functions of time. As a consequence, the quantity $I_\lambda(t)$ defined in (21) has a positive sign and can therefore be regarded as an additional recombination term.

Figure 8 compares the impact on turn-on transient time of the various model parameters. As noted in the previous section, while at low intensities the carrier mobilities significantly impact the transient time, at high intensity their effect is almost negligible if compared to that of geminate pair dynamics. The results shown are in perfect agreement with those of [25].

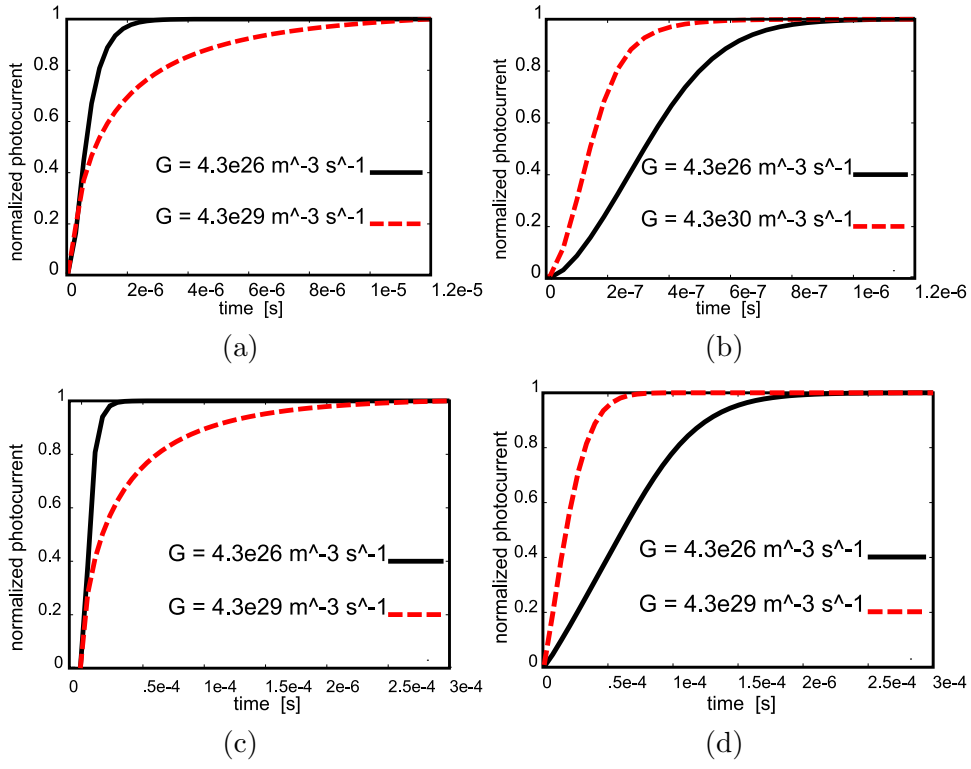

Figure 8. Transient currents at low and high intensities with different mobilities and geminate recombination rate constants. Generation rates, G , charge generation efficiencies, P, and net charge generation efficiencies, P_{net}, are shown in each case. For (a) and (b) the mobility was $2 \times 10^{-4} cm^2 V^{-1} s^{-1}$ with geminate recombination rate constants $k^{rec} = 1 \times 10^5 s^{-1}$ and $1 \times 10^7 s^{-1}$ respectively. For (c) and (d) the mobility was $2 \times 10^{-5} cm^2 V^{-1} s^{-1}$ with geminate recombination rate constants $k^{rec} = 1 \times 10^4 s^{-1}$ and $1 \times 10^6 s^{-1}$ respectively. .

6 Conclusions and Future Work

In this article, we have dealt with the mathematical modeling and numerical simulation of photocurrent transients in nanoscale mono-layer OSCs. The model consists of a system of non-linear diffusion-reaction PDEs with electrostatic convection, coupled to a kinetic ODE. We have proposed a suitable reformulation of the model which makes it similar to the drift-diffusion system for inorganic semiconductor devices. This has allowed us to prove the existence of a solution for the problem in both stationary and transient conditions and to highlight the role of exciton dynamics in determining the device turn-on time. For the numerical treatment, we carried out a temporal semi-discretization using an implicit adaptive method, and the resulting sequence of differential subproblems was linearized using the Newton-Raphson method with inexact Jacobian. Exponentially fitted finite elements were used for spatial discretization, and a thorough validation of the computational model was carried out by extensively investigating the impact of the model parameters on photocurrent transient times.

Future work is warranted in the following three main areas: 1) extensions to the model; 2) improvement of the analytical results; and 3) development of more specialized numerical algorithms. In detail:

1) we intend to include exciton transport in order to be able to simulate multi-layer or nano-structured devices [8,32,28,45];

2) we aim to extend Theorem 2 to cover the full problem (1)–(2)–(3). A possible approach to achieve this result is to apply Theorem 2 locally on a partition of $[0, T]$ into sub-intervals of size Δt, and verify the hypotheses of the Aubin lemma [26] to extract a limiting solution as $\Delta t \to 0$;

3) starting from the above idea, we intend to devise a numerical algorithm for the local approximation of the full model system over each sub-interval of size Δt using the reduced model (23)–(24). The computer implementation of this approach is straightforward as it basically amounts to a successive application of the formulation discussed in Sect. 4 on each time slab. A further improvement to the algorithm might be to improve the robustness of the non-linear solver with respect to the choice of scaling parameters (cf. Sect. 4.3) by adopting a staggered solution scheme based on some variant of Gummel's Map [21,13]. Such scheme could be either employed as an alternative to the current Newton solver or, even more effectively, combined with this latter in a predictor-corrector fashion.

7 Acknowledgements

The authors gratefully acknowledge Prof. Marco Sampietro and Dr. Dario Natali, Dipartimento di Elettronica e Informazione, Politecnico di Milano, Milano (Italy), for many helpful and stimulating discussions. They also wish to thank Prof. Joseph W. Jerome for his very careful reading of the manuscript and for his useful comments and suggestions. The first author was partially supported by the European Research Council through the FP7 Ideas Starting Grant program *"GeoPDEs – Innovative compatible discretization techniques for Partial Differential Equations"*. This support is gratefully acknowledged.

References

[1] N. Ben Abdallah, F. Mèhats, and N. Vauchelet, *A note on the long time behavior for the drift-diffusion-Poisson system*, Comptes Rendus Mathématique **339** (2004), no. 10, 683–688.

[2] R. Alley, T. Berntsen, N. L. Bindoff, Z. Chen, A. Chidthaisong, P. Friedlingstein, J. Gregory, G. Hegerl, M. Heimann, B. Hewitson, B. Hoskins, F. Joos, J. Jouzel, V. Kattsov, U. Lohmann, M. Manning, T. Matsumo, M. Molina, N. Nicholls, J. Overpeck, D. Qin, G. Raga, V. Ramaswamy, J. Ren, M. Rusticucci, S. Solomon, R. Somerville, T. F. Stocker, P. Stott, R. J. Stouffer, P. Whetton, R. A. Wood, and D. Wratt, *Climate change 2007: The physical science basis*, Tech. report, IPCC, 2007.

[3] U.M. Ascher and L.R. Petzold, *Computer methods for ordinary differential equations and differential-algebraic equations*, SIAM, 1998.

[4] Yu Bai, Yiming Cao Jing Zhang, Mingkui Wang, Renzhi Li, Peng Wang, Shaik W. Zakeeruddin, and Michael Grätzel, *High-performance dye-sensitized solar cells based on solvent-free electrolytes produced from eutectic meltscells based on solvent-free electrolytes produced from eutectic melts*, Nature Materials **7** (2008), 626–630.

[5] R. E. Bank, W. M. Coughran, and L. C. Cowsar, *Analysis of the Finite Volume Scharfetter-Gummel Method for Steady Convection Diffusion Equations.*, Computing and Visualization in Science **1** (1998), no. 3, 123– 136.

[6] F. Brezzi, L.D. Marini, and P. Pietra, *Numerical Simulation of Semiconductor Devices*, Comp. Meths. Appl. Mech. Engrg. **75** (1989), 493–514.

[7] P.N. Brown, A.C. Hindmarsh, and L.R. Petzold, *A description of DASPK: A solver for large-scale differential-algebraic systems*, Lawrence Livermore National Report UCRL (1992).

[8] G.A. Buxton and N. Clarke, *Computer simulation of polymer solar cells*, Modelling Simul. Mater. Sci. Eng. **15** (2007), 13–26.

[9] J. Campbell Scott and G.G. Malliaras, *Charge injection and recombination at the methal-organic interface*, Chemical Physics Letters **299** (1999), 115–119.

[10] S. Carl and J. W. Jerome, *Drift-diffusion in electrochemistry: Thresholds for boundary flux and discontinuous optical generation*, Applicable Analysis **83** (2004), 915–931.

[11] W. M. Coughran and J. W. Jerome, *The transient semiconductor problem with generation terms*, Modular Algorithms for Transient Semiconductor Device Simulation (ed. R.E. Bank, ed.), Lect. Appl. Math., vol. 25, American Math. Soc., Providence, 1990, pp. 107–149.

[12] C. de Falco, J. W. Jerome, and R. Sacco, *Quantum corrected drift–diffusion models: Solution fixed point map and finite element approximation*, J. Comp. Phys. **228** (2009), 1770–1789.

[13] C. de Falco, R. Sacco, and J.W. Jerome, *Quantum corrected drift–diffusion models: Solution fixed point map and finite element approximation*, J. Comput. Phys. **228** (2009), 770–1789.

[14] Kristofer Fredin, Sven Ruẗhle, Catelijne Grasso, and Anders Hagfeldt, *Studies of coupled charge transport in dye-sensitized solar cells using a numerical simulation tool*, Solar Energy Materials & Solar Cells **90** (2006), 1915–1927.

[15] S. Gabriel, B. Lutgen, B. Chakarov, M. Bursik, C. Hedegaard, M. Machnig, R. Randver, D. Roche, S. Kalogiannis, N. Ruiz, J. A. Burguette, N. Olin, A. Pecoraro Scanio, F. Fotion, G. Puhitis, A. Kundrotas, L. Lux, M. Persanyi, G. Pullicino, P. van Geel, P. Prll, J. Szyszko, F. Nunes Correia, S. Barba, J. Podobnik, J. Izak, S. Wallin, A. Carlgren, D. Miliband, I. Pearson, and S. Dimas, *Press release 2785th council meeting environment*, Tech. report, Union C. o. t. E., Ed., 2007.

[16] E. Gatti, S. Micheletti, and R. Sacco, *A New Galerkin Framework for the Drift-Diffusion Equation in Semiconductors*, East West J. Numer. Math. **6** (1998), no. 2, 101–135.

[17] W.D. Gill, *Drift mobilities in amorphous charge-transfer complexes of trinitrofluorenone and poly-n-vinylcarbazole*, J. Appl. Phys. **55** (1972), no. 12, 5033.

[18] M. Graetzel, *Solar energy conversion by dye-sensitized photovoltaic cells*, Inorg. Chem. **44** (2005), 6841–6851.

[19] Michael Grätzel, *Photoelectrochemical cells*, Nature **414** (2001).

[20] M.A. Green, *Third generation photovoltaics: Advanced solar electricity generation*, Springer-Verlag, Berlin Heidelberg, 2003.

[21] H. K. Gummel, *A Self–Consistent Iterative Scheme for One–Dimensional Steady–State Transistor Calculations*, IEEE Trans. El. Dev. **ED-11** (1964), 455–465.

[22] S. Gunes, H. Neugebauer, and N.S. Sariciftci, *Conjugated polymer-based organic solar cells*, Chem. Rev. **107** (2007), 1324–1338.

[23] E. Hairer and G. Wanner, *Solving ordinary differential equations I*, Springer Series in Computational Mathematics, Springer Verlag, Berlin, 1996.

[24] G. Horowitz, *Organic field-effect transistors*, Advanced Materials **10** (1998), no. 5, 365–377.

[25] I. Hwang and N.C. Greenham, *Modeling photocurrent transients in organic solar cells*, Nanotechnology **19** (2008), 424012 (8pp).

[26] J.W. Jerome, *Analysis of nonlinear evolution systems*, Academic Press, New York, 1983.

[27] ———, *Analysis of charge transport*, Springer-Verlag, Berlin Heidelberg, 1996.

[28] Jin Young Kim, Sun Hee Kim, Hyun-Ho Lee, Kwanghee Lee, Wanli Ma, Xiong Gong, and Alan J. Heeger, *New architecture for high-efficiency polymer photovoltaic cells using solution-based titanium oxide as an optical spacer*, Adv. Mater. **18** (2006), 572–576.

[29] R.D. Lazarov and L.T. Zikatanov, *An exponential fitting scheme for general convection–diffusion equations on tetrahedral meshes*, Comput. Appl. Math., (Obchysljuval'na ta prykladna matematyka, Kiev) **1(92)** (2005), 60–69.

[30] P.A. Markowich, *The stationary semiconductor device equations*, Springer-Verlag, Wien-New York, 1986.

[31] P.A. Markowich, C.A. Ringhofer, and C. Schmeiser, *Semiconductor equations*, Springer Verlag, Wien, 1990.

[32] A.C. Mayer, S.R. Scully, B.E. Hardin, M.W. Rowell, and M.D. McGehee, *Polymer-based solar cells*, Materials Today **10** (2007), no. 11, 28–33.

[33] V.D. Mihailetchi, L.J.A. Koster, J.C. Hummelen, and P.W.M. Blom, *Photocurrent generation in polymer-fullerene bulk heterojunctions*, Physical Review Letters **93** (2004), no. 21, 216601 (4pp).

[34] A. Quarteroni, R. Sacco, and F. Saleri, *Numerical mathematics (2nd edition)*, Texts in Applied Mathematics, vol. 37, Springer, Berlin Heidelberg New York, 2007.

[35] D.L. Scharfetter and H.K. Gummel, *Large signal analysis of a silicon Read diode oscillator.*, IEEE Trans. Electron Devices **ED-16** (1969), 64–77.

[36] T. I. Seidman, *The transient semiconductor problem with generation terms*, Computational Aspects of VLSI Design and Semiconductor Device Simulation (ed. R.E. Bank, ed.), Lect. Appl. Math., vol. 25, American Math. Soc., Providence, 1990, pp. 75–87.

[37] T. I. Seidman and G. I. Troianello, *Time–dependent solutions of a nonlinear system arising in semiconductor theory*, Nonlinear Analysis, Theory, Methods & Applications **9** (1985), no. 11, 1137–1157.

[38] S. Selberherr, *Analysis and simulation of semiconductor devices*, Springer Verlag, Wien, 1984.

[39] J.C. Simo and T.J.R. Hughes, *Computational inelasticity*, Springer–Verlag, New York, 1998.

[40] S.M. Sze and K.K. Ng, *Physics of semiconductor devices (3rd edition)*, Wiley, New York, 2006.

[41] P.E. Van Keken, D.A. Yuen, and L.R. Petzold, *DASPK: a new high order and adaptive time-integration technique with applications to mantle convection with strongly temperature-and pressure-dependent rheology*, Geophysical & Astrophysical Fluid Dynamics **80** (1995), no. 1, 57–74.

[42] D. Wrzosek, *The non-stationary semiconductor model with bounded convective velocity and generation/recombination terms*, Mathematical Modeling and Simulation of Electrical Circuits and Semiconductor Devices (R.E. Bank et al., ed.), ISNM, vol. 117, Birkhauser Verlag, Basel, 1994, pp. 293–313.

[43] ———, *Existence and uniqueness of solutions for a semiconductor device model with current dependent generation-recombination term*, Mathematical Methods in the Applied Sciences **19** (1996), no. 15, 1199–1216.

[44] H. Wu, P. A. Markowich, and S. Zheng, *Global existence and asymptotic behavior for a semiconductor drift-diffusion-Poisson model*, Mathematical Models and Methods in Applied Sciences **18** (2008), no. 3, 443–487.

[45] Dongjuan Xi, Chenjun Shi, Yan Yao, Yang Yang, and Qibing Pei, *Nanostructured polymer solar cells*, IRPS 2008, IEEE International Reliability Physics Symposium, 2008, pp. 178–180.

[46] J. Xu and L. Zikatanov, *A monotone finite element scheme for convection–diffusion equations*, Math. Comp. **68(228)** (1999), 1429–1446.